JOURNAL OF GUIDANCE, CONTROL, AND DYNAMICS
Vol. 20, No. 2, March–April 1997

Integrated Rotor-Flight Control System Optimization with Aeroelastic and Handling Qualities Constraints

Vineet Sahasrabudhe,* Roberto Celi,† and André L. Tits‡
University of Maryland, College Park, Maryland 20742

The results are presented of a study concerning the integrated optimization of rotor and flight control systems with simultaneous aeroelastic and handling qualities constraints. A representative subset of the ADS-33C handling qualities specification is reformulated into inequality constraint form. A simplified design model is used, consisting of three rotor design variables and five control system design variables for each flight condition. It is not possible to satisfy the entire set of aeroelastic and handling qualities constraints using just the three rotor design parameters of this study. If the design is optimized for just one flight condition, optimizing simultaneously the rotor and the flight control system leads to substantially better designs than by sequentially optimizing the rotor first and the flight control system next. The designs obtained using the two optimization strategies are quite different, confirming that rotor and flight control systems are strongly coupled.

Nomenclature

$\boldsymbol{A}, \boldsymbol{B}$	= state and control matrices, respectively
a_1, a_2	= roll axis pole position parameters
a_3, a_4	= pitch axis pole position parameters
a_5	= yaw axis pole position parameter
$\boldsymbol{C}(s)$	= transfer function matrix of feedforward elements
$F(\cdot)$	= objective function value
$g_j(\cdot)$	= jth constraint
$\boldsymbol{H}, \boldsymbol{H}(s)$	= matrix of feedback gains
k_ϕ, k_p	= roll attitude and rate feedback gains, respectively
k_θ, k_q	= pitch attitude and rate feedback gains, respectively
k_ψ, k_r	= yaw attitude and rate feedback gains, respectively
$L_p, L_{\theta_{1c}}$	= roll stability and control derivatives, respectively
$M(s)$	= transfer function matrix of command model
$\boldsymbol{P}$	= nonlinear plant
$\tilde{\boldsymbol{P}}^{-1}(s)$	= transfer function matrix of approximate inverse plant
p	= roll rate
R	= flap-lag elastic coupling factor
$\boldsymbol{u}$	= open-loop swashplate displacement vector
$\boldsymbol{u}_{cs}, \dot{\boldsymbol{u}}_{cs}$	= closed-loop swashplate displacement and rate vectors, respectively
$\boldsymbol{w}_1, \boldsymbol{w}_2$	= input displacement and rate weighting vectors, respectively
$\boldsymbol{X}$	= vector of design variables
$(X_i)_L, (X_i)_U$	= lower and upper bound on ith component of design vector, respectively
$\boldsymbol{x}$	= vector of states
$\Delta\boldsymbol{u}$	= perturbed input displacement vector
$\Delta\boldsymbol{x}$	= vector of perturbed states
θ_0, θ_t	= collective pitch input for main and tail rotor, respectively, rad
θ_{1s}, θ_{1c}	= longitudinal and lateral cyclic pitch input, respectively, rad
$\lambda_j(\cdot)$	= jth eigenvalue
μ	= advance ratio
$\omega_{\text{flap}}, \omega_{\text{lag}}$	= flap and lag natural frequencies, respectively, /rev

Superscripts

$(\cdot)^H, (\cdot)^{FF}$	= hover and forward flight, respectively

Received May 31, 1995; revision received June 30, 1996; accepted for publication Oct. 25, 1996.

*Research Assistant, Center for Rotorcraft Education and Research, Department of Aerospace Engineering. Student Member AIAA.

†Associate Professor, Center for Rotorcraft Education and Research, Department of Aerospace Engineering. Member AIAA.

‡Professor, Institute for Systems Research, Department of Electrical Engineering.

Introduction and Background

SUBSTANTIAL coupling between the rotor and fuselage dynamics of the fuselage may exist for helicopters equipped with hingeless and bearingless main rotors. For example, a lowly damped regressive lag mode can couple with the fuselage roll degree of freedom and result in air resonance instability. The coupling between rotor and fuselage dynamics can be further increased by the flight control system. Care must be exercised to prevent closed-loop aeroservoelastic instabilities, especially when the gains of the flight control system are high.

The possibility of interactions between rotor dynamics and a flight control system has been recognized for several decades, starting from the early work of Miller[1] and Ellis.[2] The topic was subsequently revisited by Hall and Bryson,[3] who showed that the flap regressive mode (called a rotor precession mode in Ref. 3) could be destabilized by increasing sufficiently pitch and roll attitude feedback gains.

The study by Chen and Hindson[4] combines theory with the flight testing of a variable stability CH-47 aircraft. One of the results is that increasing roll attitude feedback gains and roll rate feedback gains leads to a closed-loop instability. The same conclusion was reached by Tischler[5] in a study focusing on the BO-105. The roll attitude and roll rate feedback gains are limited by the destabilization of a coupled body roll-rotor flap regressive mode in the absence of time delays, whereas a coupled body roll-rotor lag regressive mode limits roll rate feedback gains when realistic amounts of time delay are included in the model.

In the last decade there has been an increasing interest in applying multivariable feedback control theories to the design of advanced flight control systems. A comprehensive review of this research has been presented by Manness et al.[6] The question arises of whether it is possible to neglect rotor dynamics in the design by simply lumping it with other plant uncertainties. In Ref. 7, it was suggested that this could be done using the H_∞ method. A different conclusion, however, was reached by Ingle,[8] who showed that an H_∞ based controller designed without explicitly including rotor dynamics would cause unacceptable handling qualities characteristics. Yudilevitch et al.[9] adopted a different approach to achieving handling qualities compliance using control system design. A fixed structure control

system was assumed and its parameters were varied via optimization to satisfy handling qualities specifications. A six-degree-of freedom model of the helicopter rigid-body dynamics was used, with two additional states being used to represent flap dynamics.

The research mentioned earlier, and other not mentioned for reasons of space, provides ample evidence that rotor dynamics plays a pivotal role in the design of a successful helicopter flight control system. On the other hand, in all the published studies on this topic an underlying assumption is that the rotor design is fixed. In other words, the handling qualities design objectives are achieved by operating on the architecture and on the gains of the flight control system but not on the configuration and on the design parameters of the rotor. This reflects a standard design practice, in which the rotor is designed primarily based on performance, aerodynamic, and possibly vibratory load considerations, with handling qualities a secondary objective. Although it is reasonable to assume that integrating the design of rotor and flight control systems will result in better handling qualities, simpler control systems, and much reduced risk of aeroservoelastic instabilities, there is currently little or no published information to support this assumption.

The main objective of this paper is to begin to answer the question of whether it is feasible and practical to design concurrently rotor and flight control systems and what specific benefits can be gained by such an integrated approach. This is accomplished by carrying out a numerical optimization study in which both rotor and flight control system design variables are selected to minimize control effort, subject to simultaneous aeroelastic stability and handling qualities constraints. The size of such a multidisciplinary optimization can easily become prohibitively large, thereby obscuring the fundamental features of the problem. Therefore, particular care is taken in selecting a formulation of the design problem that is simple enough that its fundamental features can be isolated and understood, but one that retains a number of underlying physical mechanisms sufficient to make it realistic.

Mathematical Model of the Helicopter

The helicopter model used for this study includes flap and lag dynamics of each blade for a four-bladed rotor, six-degree-of-freedom nonlinear fuselage dynamics and inflow dynamics. The blades are modeled as rigid blades with offset hinges and a set of springs at the root.[10] Various flap and lag frequencies can be simulated by varying the flap spring stiffness k_β, the lag spring stiffness k_ζ, and the elastic coupling parameter R.

The nonlinear coupled rotor–fuselage equations of motion are written in first-order form. The model can be used to calculate a coupled rotor–fuselage trim solution in straight flight and steady turns. The free-flight response to arbitrary pilot inputs can be simulated through integration of the nonlinear equations of motion. It is also possible to extract a linearized model by numerical perturbation of the states about the current trim position, resulting in the small perturbation equations of motion

$$\Delta \dot{\boldsymbol{x}} = \boldsymbol{A}\Delta \boldsymbol{x} + \boldsymbol{B}\Delta \boldsymbol{u} \tag{1}$$

The flight control system architecture used in this study is similar to that used in the UH-60 Advanced Digital/Optical Control System (ADOCS)[11] and is based on a model following concept. The controller structure is shown in Fig. 1. This structure consists of the nonlinear plant $\boldsymbol{P}$ (the actual helicopter), a set of simple gains $\boldsymbol{H}$ in the feedback loop, and a command model $\boldsymbol{M}$ along with a feedforward element. The feedforward element is a parallel connection of $\tilde{\boldsymbol{P}}^{-1}$, a low-order linear approximation to the inverse plant, and a gain element $\boldsymbol{H}$ identical to the one used in the feedback path. The transfer function from the desired system response δ_m to the actual output y is unity when the dynamics of the inverse plant exactly

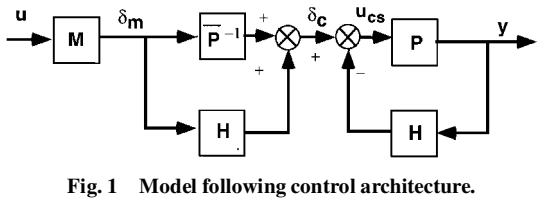

Fig. 1 Model following control architecture.

Table 1 Transfer functions of command model and inverse plant

Axis	Command model: Nominal model	Command model: Parameterized model	Inverse model
Roll	$\frac{37.5}{(s+2.5)(s+2.5)}$	$\frac{37.5}{(s+a_1)(s+a_2)}$	$\frac{(s+6.743)(s+0.241)}{58.76}$
Pitch	$\frac{24}{(s+2)(s+2)}$	$\frac{24}{(s+a_3)(s+a_4)}$	$\frac{(s+2.592)(s+0.310)}{29.87}$
Yaw	$\frac{8}{s(s+2)}$	$\frac{8}{s(s+a_5)}$	$\frac{s(s+0.381)}{7.23}$

matches that of the helicopter. Thus, by placing appropriate dynamics in the command model $\boldsymbol{M}$, any desired output can in principle be obtained at y. Feedback is applied only to the attitude loops.

The feedback matrix $\boldsymbol{H}$ consists of simple gains and is diagonal. No cross-coupling terms are present. The command model $\boldsymbol{M}$ and the inverse plant $\tilde{\boldsymbol{P}}^{-1}$ are also diagonal. The individual channel transfer functions for the command model $\boldsymbol{M}$ are given in Table 1. These transfer functions are based on Ref. 12 and reflect the desired handling qualities requirements (at least for small amplitude inputs).

The inverse plant approximation $\tilde{\boldsymbol{P}}^{-1}$ is obtained by fitting low-order transfer functions to the frequency response of each channel of a nominal linearized plant. Because the fit is of low order, the transfer function from δ_m to y is not exactly unity at all frequencies. Typically the transfer matrix $\tilde{\boldsymbol{P}}^{-1}$ thus obtained is not proper (see Table 1).

A parameterization of the controller is carried out based on the ADOCS approach.[11] First, the rate gains k_p, k_q, and k_r and the attitude gains k_ϕ, k_θ, and k_ψ in the pitch, roll, and yaw channels, respectively, are assumed to be variable. These gains are contained in the feedback matrix $\boldsymbol{H}$. Then the command model $\boldsymbol{M}$ is parameterized (see Table 1), and the poles a_1 and a_2 of the desired roll dynamics a_3 and a_4 for pitch and a_5 for yaw are assumed to be variable.

A minimal realization in first-order state space form of the control system transfer function is obtained by building a controllable realization, which is then made observable using the staircase algorithm.[13] The inverse plant $\tilde{\boldsymbol{P}}^{-1}$ is not proper and hence cannot be realized by itself. However, if we lump the feedforward elements together as $\boldsymbol{C}(s)$, we have

$$\boldsymbol{C}(s) = \tilde{\boldsymbol{P}}^{-1}(s)\boldsymbol{M}(s) + \boldsymbol{H}(s)\boldsymbol{M}(s) \tag{2}$$

This feedforward element $\boldsymbol{C}(s)$ is now realizable if $\tilde{\boldsymbol{P}}^{-1}(s)\boldsymbol{M}(s)$ is proper.

Formulation of the Optimization Problem

The optimization problem is formulated in nonlinear mathematical programming form. Thus we seek a vector $\boldsymbol{X}$ of design variables that minimizes an objective function $F(\boldsymbol{X})$, subject to behavior constraints of the type $g_j(\boldsymbol{X}) \le 0$, $j = 1, \ldots, m$, and side constraints $(X_i)_L \le X_i \le (X_i)_U$, $i = 1, \ldots, n$, where m is the total number of constraints, n is the number of design variables, $(X_i)_L$ is the lower limit on design variable X_i, and $(X_i)_U$ is the upper limit on X_i.

Two optimization strategies were used. In the first, which we call sequential optimization, the rotor design variables were optimized first for a bare airframe configuration. The rotor design was then frozen, and the control system was optimized. The second strategy, which we call integrated optimization, consisted of optimizing both rotor and control system simultaneously. The overall organization of the optimization process is shown in Fig. 2.

Aeroelastic Constraints

The aeroelastic constraints enforce rotor aeroelastic stability by requiring that the real parts of the eigenvalues λ_j of the state matrix $\boldsymbol{A}$ corresponding to the rotor modes be negative. For a 4-bladed rotor with independent flap and lag degrees of freedom there will be 16 stability eigenvalues. If a constant coefficient representation of the state matrix is used, as in this study, the eigenvalues will appear in complex conjugate pairs. In this case there would only be eight independent complex conjugate pairs. The model of the helicopter used in this study is not likely to predict the rotor vibratory loads with sufficient accuracy. Therefore, no rotor loads constraints were included in the optimization.

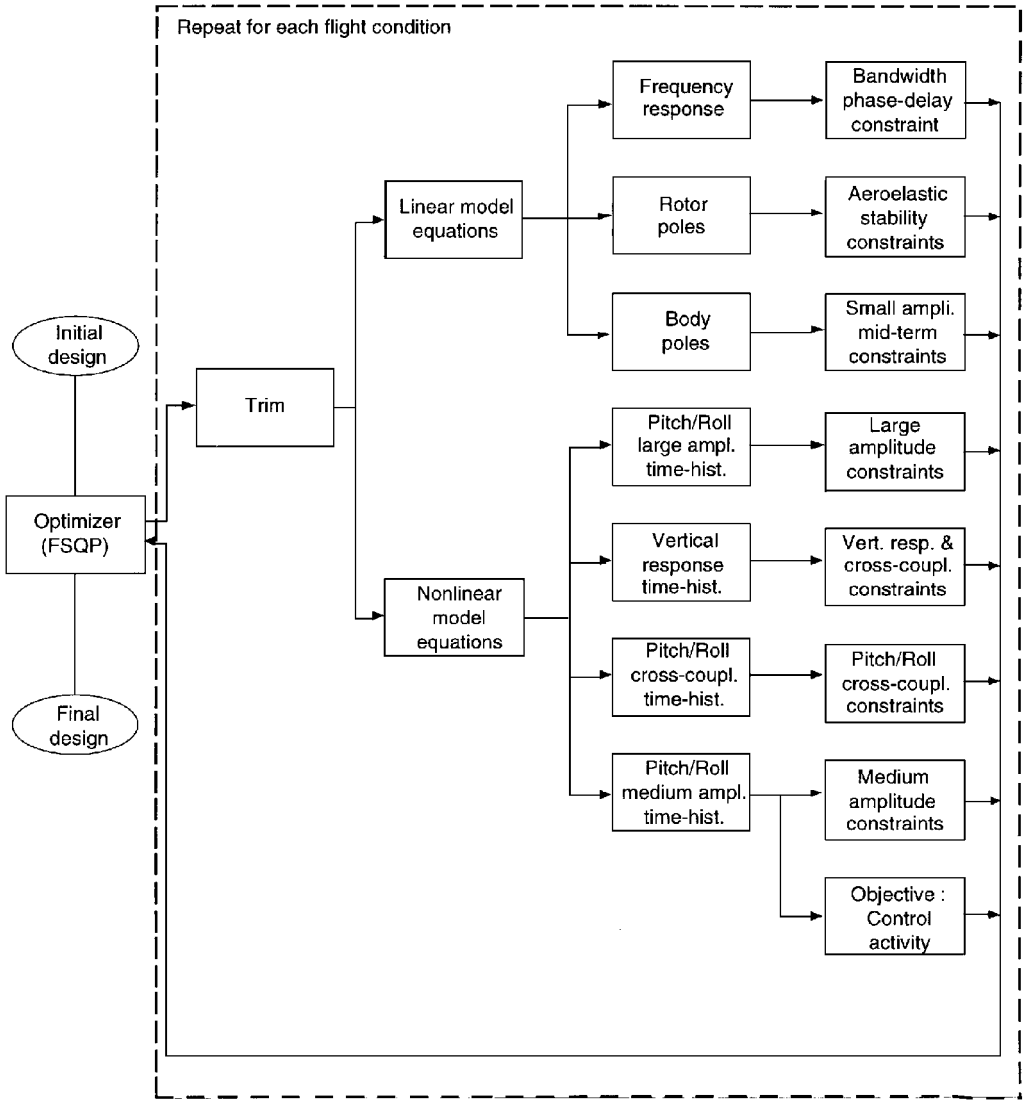

Fig. 2 Organization of optimization process.

Handling Qualities Constraints

The handling qualities constraints enforce compliance with a representative subset of the ADS-33 specifications[14] for hover. The following specifications were chosen to formulate the constraints. Bandwidth-phase delay constraints (Spec. 3.3.2.1 of ADS-33) for roll and pitch: these are constraints on the shape of the frequency response. Damping constraints (3.3.2.2) for the phugoid, Dutch roll, roll, and pitch poles: these are pole placement type constraints. Attitude quickness (3.3.3) constraints in pitch and roll; large amplitude (3.3.4) constraints on roll, pitch, and yaw attitudes and rates; vertical response (3.3.10.1) constraints; interaxis-coupling (3.3.9) constraints on yaw-due-to-collective, roll-to-pitch, and pitch-to-roll coupling: all these are constraints on the time histories of the response to pilot inputs.

For the bandwidth-phase delay specifications, the frequency response of this system is calculated from Eq. (1) and the bandwidth and phase-delay values were then determined as described in ADS-33 (Ref. 14). The eigenvalues of the linearized model are also used for the pole placement specifications.

For the moderate amplitude specifications, a desired time history attitude response was assumed and the corresponding rate was obtained by differentiation. The dynamics were then modeled using simple one degree-of-freedom linear equations and solving for the required input. For the roll degree of freedom, this results in

$$\theta_{1c}(t) = \frac{\dot{p}(t) - L_p p(t)}{L_{\theta_{1c}}} \tag{3}$$

This input was then applied to the full nonlinear system model and the attitude response obtained by integrating the equations of motion. The output was usually not exactly the same as the output of the simple linear models, but it was of the same general form and adequate for the evaluation of the handling qualities characteristics. Only one time history, that is, only one value of attitude change, was used for each specification. This is sufficient to study the basic effects of these requirements on the entire optimization problem. On the other hand, it should not be considered as a complete verification of compliance with the quickness specifications. In fact, this would require a number of time histories sufficient to cover the entire range of values of attitude changes included in each specification.

The large amplitude specification was evaluated by using a scaled version of the moderate amplitude input. The vertical response specification and the yaw-due-to-collective specification require a step collective input. A first-order system response was fitted to the vertical rate response as required by Ref. 14, and the fit parameters were used for the specification. Finally, the pitch/roll cross-coupling specifications were evaluated by feeding a step input to each of the axes in turn and comparing the on- and off-axis responses.

Many of the handling qualities specifications are expressed in graphical form, as boundaries of regions in which the points representative of the helicopter must fall to achieve certain handling qualities levels. The specifications were transformed into inequality constraints by calculating the distance of the representative point P from the prescribed boundary L on the appropriate specification plot (Fig. 3). A negative sign was assigned to the distance if the desired handling qualities level was achieved, and a positive sign if

it was not. This distance was used as the constraint value g_j. Unless specified otherwise, all the constraints in the present study are based on level 1 requirements. The 18 handling qualities constraints were added to the 8 aeroelastic constraints for a total of 26 constraints.

Sequential Optimization

The sequential optimization consists of two phases: a rotor optimization followed by a flight control system optimization.

Step 1—Rotor Only

The design vector $\boldsymbol{X}$ for the rotor optimization phase simply consisted of the rotor stiffness parameters k_β and k_ζ and the elastic coupling factor R. Thus,

$$\boldsymbol{X} = [k_\beta, k_\zeta, R]^T \tag{4}$$

Only a bare airframe configuration was assumed in this phase. It was not usually possible to obtain a feasible solution without a flight control system. Therefore, the objective function was formulated as the sum of the values of the violated constraints. Hence,

$$F(\boldsymbol{X}) = \sum g_j(\boldsymbol{X}), \qquad j = 1, \ldots, n_V \tag{5}$$

where n_V is the total number of violated constraints and all the g_j are positive because they correspond to violated constraints. Thus the objective of the first phase of the optimization was to design an aeroelastically stable rotor and to satisfy as many handling qualities constraints as possible by reducing the value of $F(\boldsymbol{X})$, possibly to zero.

Step 2—Flight Control System Only

For this step the rotor configuration was held fixed at the optimum of step 1, and the flight control system was optimized. The design vector for the control optimization consisted only of the control system parameters. To reduce the number of design variables, design variable linking was used. Thus attitude and rate gains for roll and yaw were set to be identical, that is, $k_p = k_\phi$ and $k_r = k_\psi$. Similarly, the roll and pitch pole variables were linked by setting $a_1 = a_2$ and $a_3 = a_4$. (It should be noted that this choice has the effect of forcing the damping ratio in both roll and pitch to be equal to one.) Finally, the yaw pole variable a_5 was held fixed at its nominal value of 1.99 rad/s. Hence, the design variable vector actually used was

$$\boldsymbol{X} = [k_p, k_q, k_r, k_\theta, a_1, a_3]^T$$

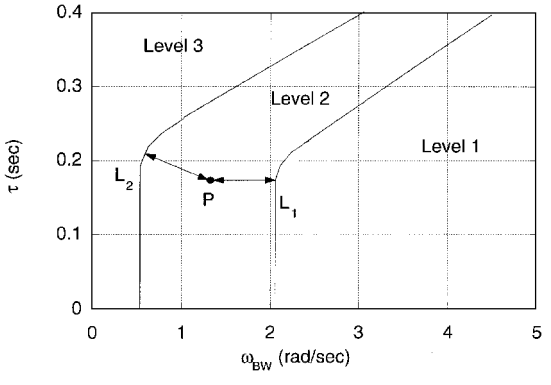

Fig. 3 Handling qualities constraint definition for small amplitude short term specification in pitch (hover).

For the control system optimization phase, the objective function was chosen to be a weighted sum of the swashplate displacement and rate vectors ($\boldsymbol{u}_{cs}$ and $\dot{\boldsymbol{u}}_{cs}$), for two predefined maneuvers, namely, those used to evaluate compliance with Specification 3.3.3 in roll and pitch. Figure 1 clarifies the relationship between $\boldsymbol{u}_{cs}$ and the plant input vector $\boldsymbol{u}$ defined earlier. Thus $\boldsymbol{u}_{cs}$ is the closed-loop input vector to the helicopter when the control system has been introduced, and $\dot{\boldsymbol{u}}_{cs}$ is the time derivative of $\boldsymbol{u}_{cs}$. The vectors $\boldsymbol{u}_{cs}$ and $\dot{\boldsymbol{u}}_{cs}$ are representative of the inputs that would go into swashplate actuators. Hence minimization of an objective function based on these displacements and rates is equivalent to minimizing inputs to actuators placed at that point. The objective function was defined as

$$F(\boldsymbol{X}) = \sum \int_0^T \left[\boldsymbol{w}_1^T \boldsymbol{u}_{cs}(t, \boldsymbol{X})^2 + \boldsymbol{w}_2^T \dot{\boldsymbol{u}}_{cs}(t, \boldsymbol{X})^2\right] \mathrm{d}t \tag{6}$$

where $\boldsymbol{w}_1$ and $\boldsymbol{w}_2$ are weighting vectors, and the summation is carried out over the two different maneuvers. The objective $F(\boldsymbol{X})$ is a measure of control activity at the actuator inputs. The constraints used for the control optimization were identical to those of step 1.

Integrated Optimization

The design vector for this case consisted of both the rotor and control system parameters used in the sequential optimization procedure. Thus,

$$\boldsymbol{X} = [k_\beta, k_\zeta, R, k_p, k_q, k_r, k_\theta, a_1, a_3]^T$$

The objective function used was the control activity measure given in Eq. (6). The same set of constraints as in the sequential optimization was used in this case.

Results and Discussion

The results presented in this section are for a hingeless rotor with solidity $\sigma = 0.07$. The angular velocity of the rotor is 424 rpm. The weight coefficient is $C_W = 0.005$. The rotor has four blades and the blade airfoil has a lift curve slope of $a = 6.0$ and a profile drag coefficient $c_{d_0} = 0.01$. The fuselage gross weight is 4855 lb. The c.g. of the aircraft is $0.2R$ below the hub. Both the sequential and the integrated optimization procedures were carried out starting from the initial designs defined in Table 2. The numbers in parentheses are the flap and lag frequencies corresponding to the spring stiffnesses and coupling parameter R. The initial design is typical of a soft-in-plane hingeless rotor.

Sequential Optimization

Step 1—Rotor Only, No Flight Control System

No feasible initial solution was obtained for this problem. The violated constraints were the three constraints associated with interaxis coupling and the phugoid pole placement constraint. Preliminary sensitivity studies showed that the phugoid poles cannot be appreciably modified using the rotor design parameters of this study. Hence the phugoid constraint was arbitrarily relaxed so that it

Table 2 Design variables: initial and final values

Design variable	Sequential optimization				Integrated optimization	
	Rotor initial	Rotor final	Control initial	Control final	Initial	Final
$k_\beta \times 5.0e{-}05$	10.78 (1.12)	10.111 (1.115)	——	——	10.78 (1.12)	10.744 (1.119)
$k_\zeta \times 5.0e{-}06$	2.494 (0.70)	2.592 (0.71)	——	——	2.494 (0.70)	2.689 (0.72)
R	0.9	0.0	——	——	0.9	0.898
k_p, k_ϕ	——	——	−0.0288	−0.0288	−0.0288	−0.0398
k_q	——	——	0.5332	0.5332	0.5332	0.3546
k_θ	——	——	0.0692	0.0689	0.0692	0.0619
k_r, k_ψ	——	——	−0.0194	−0.0194	−0.0194	−0.0376
a_1, a_2	——	——	0.8827	0.8827	0.8827	0.6125
a_3, a_4	——	——	0.7982	0.7986	0.7982	0.8435

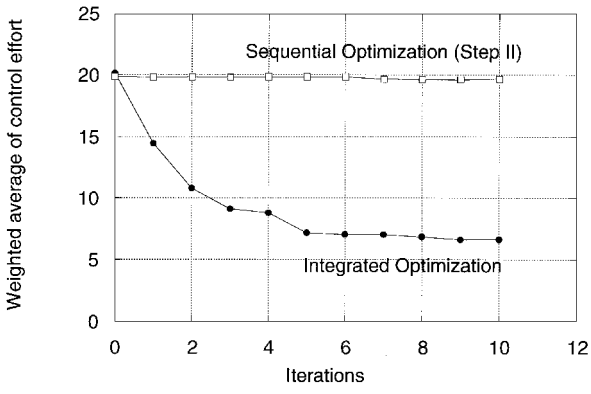

Fig. 4 Objective function iteration history: sequential vs integrated optimization.

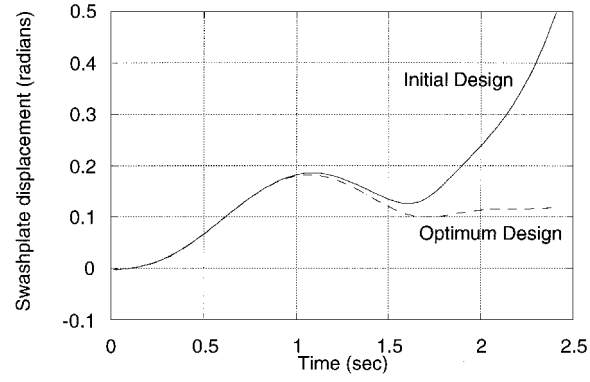

Fig. 5 Swashplate displacement during moderate amplitude pitch maneuver for initial and final design (integrated optimization).

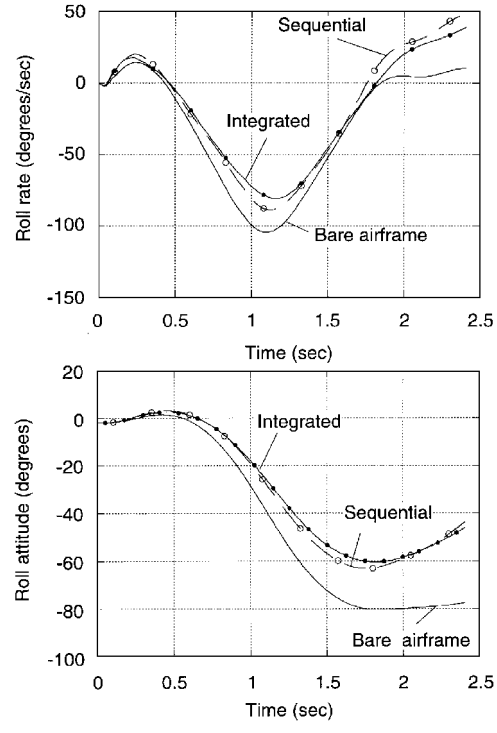

Fig. 6 Moderate amplitude roll rate and roll attitude response of various designs.

was satisfied by the initial design. However, the preliminary studies indicated that the violation of the cross-coupling constraints could be reduced using the selected rotor design parameters. The cross-coupling constraints were relaxed so that the optimizer could start from a feasible design, but they were also included in the objective function. With this formulation of the design problem, the optimizer tried to minimize the cumulative violation of the original cross-coupling constraints. The final optimum design was still infeasible for the original set of unrelaxed constraints. The final design values are shown in the second column of Table 2.

Comparing the initial and the final design, it is obvious that the major change that has taken place is in the value of the coupling parameter R. The value of R decreases from the starting value of 0.9 to 0.0. This corresponds to a rotor with all its flexibility inboard of the pitch bearing. Results not presented here indicate the violation of this constraint can be reduced slightly, but not eliminated, by lowering the value of R.

Step 2—Flight Control System Only

The initial design for the second phase of the sequential optimization was the optimized rotor obtained at the end of step 1. The initial values of the design variables that describe the flight control system are shown in Table 2. This initial design was obtained through a small amount of trial and error. This design satisfies all constraints except the phugoid level 1 constraint, but designs that violated more constraints would have also been acceptable.

With the addition of a flight control system it was possible to obtain a feasible design without having to relax any constraint. Therefore the flight control system optimization was carried out with the more stringent control activity objective function defined in Eq. (6). The iteration history of the objective function is shown in Fig. 4. Clearly, although feasible designs are achieved, a sequential optimization strategy does not significantly reduce control effort. In fact, the objective function only showed a decrease of less than 1%.

Integrated Optimization

The initial design for the integrated optimization consists of the initial rotor parameters for step 1 and the initial flight control system parameters for step 2 of the sequential optimization. The initial values are listed in the fifth column of Table 2. The initial design is feasible.

The iteration history of the objective function for this case is shown in Fig. 4. At the end of the optimization the control activity was reduced by 67% and all the constraints were satisfied. This reduction was significantly larger than that obtained by sequential optimization. Figure 5 shows the improvement in swashplate input displacement for the moderate amplitude pitch maneuver, for both the initial and the optimized design. The reduction in control activity is clearly evident, especially in the later phases of the maneuver.

The roll rate and attitude responses to a shaped lateral input are shown in Fig. 6. These responses were used to calculate the value of the roll attitude quickness specification. The optimization produced designs such that both attitude and roll peaks were lower than their initial values. However, the ratio of peaks was such that the constraint was still satisfied. Figure 7 shows the pitch and roll attitude responses to a longitudinal cyclic step input. The figure clearly shows the improvement in the roll due to pitch cross-coupling as a result of optimization. The final design obtained by integrated optimization had marginally lower cross-coupling than that obtained by simultaneous optimization. Finally, the yaw rate response due to collective input is shown in Fig. 8. Once again the optimal designs had a much lower off-axis response, with both the simultaneous and integrated optimization producing comparable reductions.

The final rotor design obtained from the integrated design procedure is listed in the last column of Table 2. Compared with the sequentially optimized design, the flap and lag stiffnesses change by similarly small amounts, but the elastic coupling parameter R is substantially different. The optimum value of $R = 0.898$ corresponds to a rotor with most of the bending flexibility outboard of the pitch bearing and therefore with a large virtual hinge offset.

The likely reason for the different optimum values of R in the two final designs is the following. With a sequential optimization strategy, when the optimizer is selecting the rotor parameters, it cannot take advantage of the flight control system because in the first step there are no control design variables. Therefore it attempts to reduce the cross-couplings by essentially reducing the virtual hinge offset through a small value of R. On the other hand, when rotor and flight control system parameters are available simultaneously

Table 3 Off-design performance for various rotor/control combinations

Design	Control activity, from Eq. (6)
Baseline (bare airframe)	89.97
Baseline with initial controller	89.64
Optimized (sequential)	229.30
Optimized (integrated)	49.54

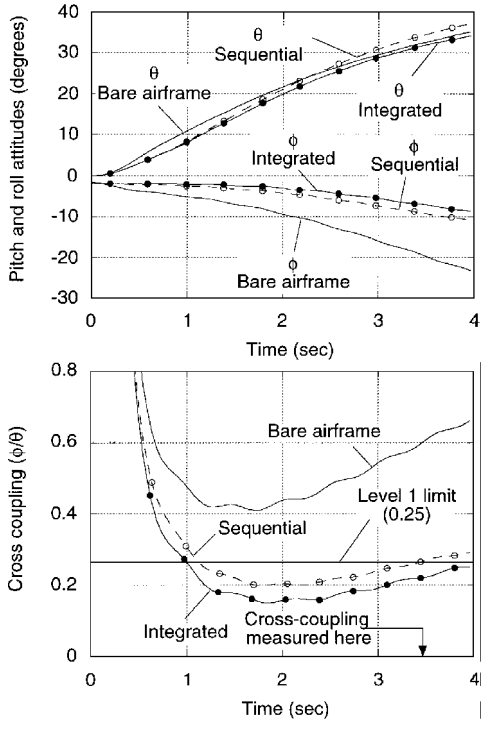

Fig. 7 Pitch and roll attitude response and interaxis coupling due to lateral step input.

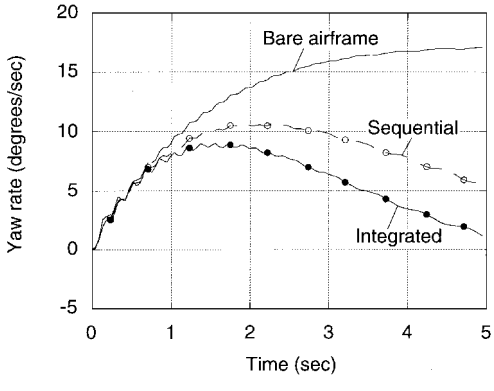

Fig. 8 Yaw rate response to collective input.

for the optimization, the latter are used as the primary means to satisfy the cross-coupling constraints.

Off-Design Analysis

Both optimal configurations were also analyzed in an off-design flight condition, namely forward flight at an advance ratio $\mu = 0.15$. These configurations were compared with two baseline designs at the same flight condition. The first baseline design corresponds to the unoptimized rotor and control combination in the fifth column of Table 2. The second baseline design corresponds to the optimized rotor in the second column of the table in combination with the control variable values in the third column of the table, that is, the initial design for step 2 of the sequential optimization.

Table 3 shows the control activities of these designs. The optimum rotor/flight control design obtained using the integrated optimization procedure appears to have a lower control activity in the off-design conditions as well. However, it is infeasible and violates the pitch and roll moderate amplitude constraints, and the pitch-to-roll and roll-to-pitch cross-coupling constraints. The sequentially optimized design, in the off-design condition, violates the roll pole-placement constraint, the roll moderate amplitude constraint, and the roll-to-pitch cross-coupling constraint. The two baseline designs, on the other hand, are feasible.

Two-Point Optimization

The off-design analysis showed that the optimized configurations do not perform adequately in off-design, forward-flight conditions, because the control activity is higher than the baseline and/or several of the constraints are violated. As a way of making the design satisfactory over a broader range of advance ratios, a two-point optimization was carried out. The two flight conditions chosen were hover and forward flight at an advance ratio of $\mu = 0.15$. Thus the design variables consisted of one set of rotor design variables and two sets of control design variables, one each for hover and forward flight, for a total of 15 design variables. Both the sequential and the integrated optimization strategies were employed.

For the sequential optimization the structural optimization phase (step 1) has the same three-element vector of design variables as in Eq. (4). The constraint set, however, consists of constraints at both hover and forward flight. The handling qualities constraints associated with the forward-flight specifications are defined in the same way as in the hover case, that is, as distances of the point representative of the aircraft from the boundary of the handling qualities level 1. The following specifications were used for the forward-flight case. Bandwidth-phase delay constraints for roll (Spec. 3.4.5.1 of Ref. 14) and pitch (3.4.1.1): these are constraints on the shape of the frequency response. Damping constraints (3.4.1.2 and 3.4.5.1) for the phugoid, Dutch roll, roll, and pitch poles: these are pole-placement type constraints. Attitude quickness constraints in pitch (same as hover) and roll (3.4.5.2); large amplitude constraints on roll (3.4.5.3) and pitch (same as hover) attitudes and rates; interaxis-coupling (3.4.4.2) constraints on roll-to-pitch and pitch-to-roll coupling: all these are constraints on the time histories of the response to pilot inputs. This gives a total of 14 handling qualities constraints in forward flight. The periodicity of the state matrix in forward flight was ignored in this study and a constant coefficient approximation was used, resulting in eight aeroelastic stability constraints.

The objective function for step 1 of the sequential optimization procedure was the sum of the violated constraints as defined in Eq. (5). The violated constraints included in the objective function were the pitch/roll cross-coupling constraints in hover and forward flight, the yaw-due-to-collective cross-coupling in hover, and the pitch moderate amplitude constraint in forward flight. There was no appreciable improvement in the objective function. Initial and final values of the rotor design variables are listed in Table 4.

The control optimization phase (step 2 of the sequential approach) consists of optimizing two sets of parameters, one each for hover and forward flight. The constraint set included both hover and forward-flight constraints. Because the rotor design is kept frozen in this phase, this problem can be decoupled into two independent, smaller subproblems, one for each flight condition. The hover problem consists of the hover set of control design variables and the hover constraints; similarly, for the forward-flight condition. For both flight conditions, the objective function was the measure of control activity as defined by Eq. (6). Figure 9 shows the iteration history of the objective function. The initial and final values of the control design variables are listed in Table 4. These values were obtained from a small amount of trial and error. The design vector for the integrated optimization approach is

$$\boldsymbol{X} = \left[k_\beta, k_\zeta, R, k_p^H, k_q^H, k_r^H, k_\theta^H, a_1^H, a_3^H,\right.$$
$$\left. k_p^{FF}, k_q^{FF}, k_r^{FF}, k_\theta^{FF}, a_1^{FF}, a_3^{FF}\right]^T$$

Because the rotor design was being varied simultaneously with the flight control system, it was not possible to decouple the problem into hover and forward flight subproblems and it was necessary to consider both hover and forward-flight constraints. Hence, there

Table 4 Two-point optimization: design variables—initial and final values

Design variable	Sequential optimization				Integrated optimization	
	Rotor initial	Rotor final	Control initial	Control final	Initial	Final
$k_\beta \times 5.0e{-}05$	10.78 (1.12)	10.895 (1.121)	——	——	10.78 (1.12)	12.078(1.13)
$k_\zeta \times 5.0e{-}06$	2.494 (0.70)	2.493 (0.70)	——	——	2.494 (0.70)	2.6096(0.71)
R	0.9	0.899	——	——	0.9	0.6289
k_p^H, k_ϕ^H	——	——	−0.0288	−0.040	−0.0288	−0.032
k_q^H	——	——	0.5332	0.453	0.5332	0.275
k_θ^H	——	——	0.0692	0.036	0.0692	0.023
k_r^H, k_ψ^H	——	——	−0.0194	−0.0375	−0.0194	−0.018
a_1^H, a_2^H	——	——	0.8827	0.557	0.8827	0.696
a_3^H, a_4^H	——	——	0.7982	1.033	0.7982	0.925
k_p^{FF}, k_ϕ^{FF}	——	——	−0.0188	−0.004	−0.0188	0.018
k_q^{FF}	——	——	0.732	0.376	0.732	0.287
k_θ^{FF}	——	——	0.0689	0.042	0.0689	0.012
k_r^{FF}, k_ψ^{FF}	——	——	−0.0194	0.041	−0.0194	−0.04
a_1^{FF}, a_2^{FF}	——	——	0.9827	1.333	0.9827	1.523
a_3^{FF}, a_4^{FF}	——	——	0.8986	0.822	0.8986	0.930

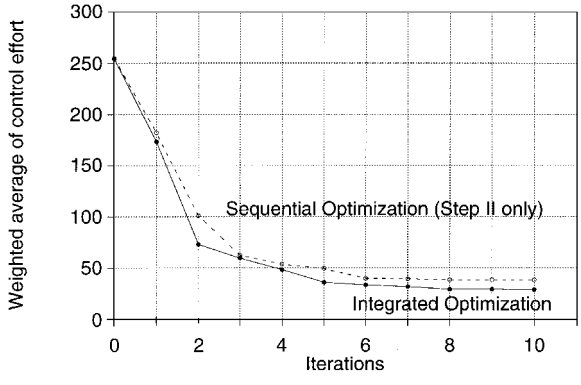

Fig. 9 Objective function: two-point integrated optimization.

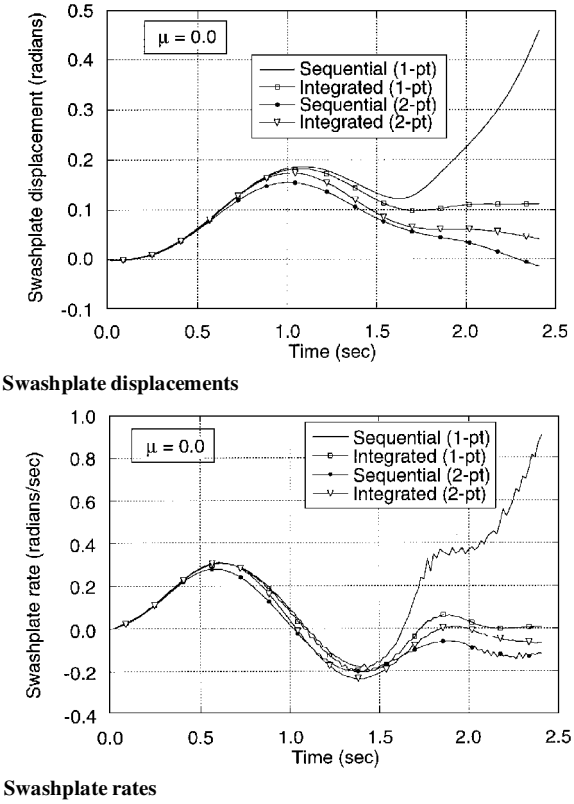

a) Swashplate displacements

b) Swashplate rates

Fig. 10 Swashplate displacements and rates during moderate amplitude pitch maneuver.

were a total of 48 constraints. Figure 9 shows the iteration history of the objective function for both the integrated approach and the sequential approach. The objective functions here include the control activity in both hover and forward flight. The final value obtained using an integrated optimization approach is almost 25% lower than the best value obtained using the sequential optimization procedure. Thus, the benefits of an integrated optimization over a sequential one do not appear as significant as they did for the single point optimization. A possible explanation lies in the value of the flap-lag elastic coupling factor R. It is clear from the integrated optimization results that the best value of R is between 0.6 and 0.9, depending on the specific problem. The rotor-only portion of the sequential optimization in hover ended with a final value of $R = 0$, which was held constant in the subsequent flight control system-only phase. This means that the optimizer had to work with a rotor that we know a posteriori not to be a very good configuration. Consider now the sequential optimization for the two-advance ratio case. At the end of the rotor-only phase, the value of R is about 0.9. Thus phase 2 will start from a much better design than it did in the previous case. Therefore, the sequential optimum design will be better than in the single advance ratio case, and it is not surprising that the improvement produced by an integrated optimization is smaller than in the single μ case.

Figures 10a and 10b show, respectively, the time history of the swashplate input displacements and rates for a moderate amplitude pitch maneuver in hover. The one- and two-point sequential and integrated designs are compared. In the maneuvers required to evaluate compliance with the quickness specification, actuator rate and displacement saturation may sometime occur. Such effects have been neglected in the present study. Figure 11 shows that saturation is likely to occur only in the one-point sequentially optimized design. For the three other optimum designs, an objective function of the form of Eq. (13) proves effective in reducing control activity to the point that saturation becomes unlikely.

Off-Design Analysis for Two-Point Optimization

The two-point rotor design process described earlier optimized rotor and flight control systems for both hover and forward flight at $\mu = 0.15$. All level 1 handling qualities requirements were met at both speeds and stability was maintained.

An off-design analysis was performed by considering forward flight speeds of $\mu = 0.1$ and 0.2. Both hover and forward flight gains were used for $\mu = 0.1$, and forward flight gains were used for $\mu = 0.2$. Table 5 shows the value of the objective function used in the optimization for three different cases. In the first case, the advance ratio is $\mu = 0.1$ and the flight control system gains are those optimal for hover. In the second case, $\mu = 0.1$ but the gains are optimal for

Table 5 Off-design analysis for two-point optimum designs

Case	Control activity, from Eq. (6)	
	Sequential design	Integrated design
$\mu = 0.1$ with hover controller	16.96	21.18
$\mu = 0.1$ with forward-flight controller	25.06	65.84
$\mu = 0.2$ with forward-flight controller	327.47	101.31

$\mu = 0.15$. In both cases, optimizing rotor and flight control systems simultaneously rather than sequentially leads to reduced control effort. The reverse, however, seems to be true for the off-design flight condition $\mu = 0.2$, in which the flight control system gains are those optimal for $\mu = 0.15$. The pitch-to-roll cross-coupling constraint is not satisfied for any of the off-design conditions. In addition, at least one other constraint is violated in each case, namely, the roll medium amplitude constraint for the $\mu = 0.1$/hover gain case, the roll medium amplitude constraint for the $\mu = 0.1$/forward-flight gain case, and the roll-to-pitch cross coupling constraint for the $\mu = 0.2$/forward-flight gain case for designs obtained by the sequential optimization procedure. In the off-design analysis of the integrated optimization design, the pitch/roll cross-coupling constraints and the roll moderate amplitude constraint are violated in each of the three cases mentioned earlier. Thus, one or more constraints are violated in each of the off-design flight conditions, indicating that steps should be taken to improve the robustness of the optimum designs.

Summary and Conclusions

This paper contains the results of a study concerning the integrated optimization of a rotor and flight control system subject to simultaneous aeroelastic and handling qualities constraints. A representative subset of the ADS-33 handling qualities specifications was reformulated into inequality constraint form so as to be compatible with numerical optimization procedures. A simplified design model was used, consisting of three rotor design variables and five control system design variables for each flight condition.

The main results of the study are the following:

1) It is not possible to satisfy the entire set of aeroelastic and handling qualities constraints using just the three rotor design parameters of this study. It is likely, however, that the same conclusion would hold even if more rotor design parameters were available. The constraints on the off-axis response to the pilot inputs are the most difficult to satisfy.

2) If the design is optimized for just one flight condition, optimizing simultaneously rotor and flight control systems leads to substantially better designs than by sequentially optimizing the rotor first and the flight control system next. Both designs satisfy all the constraints, but the integrated optimization produces designs with far lower control effort requirements. The designs obtained using the two optimization strategies are quite different, confirming that the rotor and flight control systems are strongly coupled. In off-design flight conditions, the integrated optimum designs tend to perform better than sequentially optimized designs, but both types of designs become infeasible.

3) If the design is optimized for more than one flight condition, optimizing simultaneously rotor and flight control systems still leads to better designs than a sequential optimization approach in terms of control activity, although the improvements are smaller than in the single-point case. The off-design behavior appears to be better than that of the sequentially optimized designs for flight conditions within (but not outside) those actually used for the optimization. It also appears to be better than for the designs optimized for just one flight condition. However, one or more constraints are violated by each design in each of the off-design flight conditions, indicating that steps should be taken to improve the robustness of the optimum designs.

Acknowledgments

The authors acknowledge the support for this research work by the U.S. Army Research Office under the Center for Rotorcraft Education and Research Contract DAAH-04-94-G-0074; the Technical Monitor was Tom Doligalski. An earlier version of this paper was presented at the American Helicopter Society 51st Annual Forum, Fort Worth, Texas, May 11–13, 1995.

References

[1]Miller, R. H., "A Method for Improving the Inherent Stability and Control Characteristics of Helicopters," *Journal of the Aeronautical Sciences*, Vol. 17, June 1950, pp. 363–374.

[2]Ellis, C. W., "Effect of Articulated Rotor Dynamics on Helicopter Automatic Control System Requirements," *Aeronautical Engineering Review*, Vol. 12, July 1953, pp. 30–38.

[3]Hall, W. E., Jr., and Bryson, A. E., Jr., "Inclusion of Rotor Dynamics in Controller Design for Helicopters," *Journal of Aircraft*, Vol. 10, No. 4, 1973, pp. 200–206.

[4]Chen, R. T. N., and Hindson, W. S., "Influence of High-Order Dynamics on Helicopter Flight-Control Bandwidth," *Journal of Guidance, Control, and Dynamics*, Vol. 9, No. 2, 1986, pp. 190–197.

[5]Tischler, M. B., "System Identification Requirements for High-Bandwidth Rotorcraft Flight Control System Design," *Journal of Guidance, Control, and Dynamics*, Vol. 13, No. 5, 1990, pp. 835–841.

[6]Manness, M. A., Gribble, J. J., and Murray-Smith, D. J., "Multivariable Methods for Helicopter Flight Control Law Design: A Review," Seventeenth European Rotorcraft Forum, Paper III.5.2, Glasgow, Scotland, UK, Sept. 1990.

[7]Yue, A., and Postlethwaite, I., "Robust Helicopter Control Laws for Handling Qualities Enhancement," Royal Aeronautical Society Conference on Helicopter Handling Qualities and Control, Paper 14, London, Nov. 1988.

[8]Ingle, S. J., "The Effect of Higher Order Dynamics on Helicopter Flight Control Law Design," M.S. Thesis, Dept. of Aerospace Engineering, Univ. of Maryland, College Park, MD, July 1991.

[9]Yudilevitch, G., and Levine, W. S., "Rotorcraft Flight Control System Design Using CONSOL-OPTCAD—Final Report," Inst. for Systems Research, ISR TR-94-54, Univ. of Maryland, College Park, MD, 1994.

[10]Ormiston, R. A., and Hodges, D. H., "Linear Flap-Lag Dynamics of Hingeless Helicopter Rotor Blades in Hover," *Journal of the American Helicopter Society*, Vol. 17, No. 2, 1972, pp. 2–14.

[11]Landis, K. H., and Glusman, S. I., "Development of ADOCS Controllers and Control Laws," NASA CR 177339, 1984.

[12]Tischler, M. B., Fletcher, J. W., Morris, P. M., and Tucker, G. E., "Flying Quality Analysis and Flight Evaluation of a Highly Augumented Combat Rotorcraft," *Journal of Guidance, Control, and Dynamics*, Vol. 14, No. 5, 1991, pp. 954–963.

[13]Maciejowski, J. M., *Multivariable Feedback Design*, Addison–Wesley, Reading, MA, 1989.

[14]Hoh, R. H., Mitchell, D. G., Aponso, B. L., Key, D. L., and Blanken, C. L., "Handling Qualities Requirements for Military Rotorcraft," STI TR 1194-6, Systems Technology, Inc., 1989.